SPIN
Vol. 7, No. 3 (2017) 1740013 (14 pages)

DOI: 10.1142/S2010324717400136

World Scientific
www.worldscientific.com

Spin–Orbit Torques in Metallic Magnetic Multilayers: Challenges and New Opportunities

Tao Wang*, John Q. Xiao* and Xin Fan†,‡
*Department of Physics and Astronomy
University of Delaware, Newark, DE 19716, USA
†Department of Physics and Astronomy
University of Denver, Denver, CO 80210, USA
‡xin.fan@du.edu

Received 16 June 2017
Accepted 24 July 2017
Published 25 August 2017

Two decades after the discovery of the giant magnetoresistance that revolutionizes the hard disk drive, the rapid development of spin torque-based magnetic random access memory has once again demonstrated the great potential of spintronics in practical applications. While the industrial application is mainly focusing on the implementation of current-induced spin transfer torque (STT) in magnetic tunnel junctions, a new type of spin torque emerges due to the spin–orbit interaction in magnetic multilayers. A great effort has been devoted by the scientific community to study the so-called spin–orbit torque (SOT), which is not only of interest to fundamental science, but also exhibits potential for the application of current-induced magnetization switching. In this paper, we will review recent development in the SOTs including the fundamental understanding, materials development and measurement techniques. We will also discuss the challenges of using the SOT in potential applications, particularly on the switching of perpendicularly magnetized films.

Keywords: Spin–orbit torque; spin Hall effect; Rashba–Edelstein effect; magnetic random access memory.

1. Introduction of Spin–Orbit Torques and their Potential Applications

Along with the fast development of computers, there has been an ever-increasing demand for information storage technologies that are fast, nonvolatile and with low energy consumption.[1] Among various types of techniques, magnetism is one of the most popular choices as the information storing medium due to its high stability and scalability.[2–5] Over the past three decades, the rapid development in the hard disk drives and more recently, the magnetic random access memories (MRAMs) are remarkable examples for how fundamental research in magnetism can impact different types of applications in information storage. The discovery of the giant magnetoresistance effect,[6,7] which describes how magnetization can influence the charge transport, has led to significant breakthroughs of read heads in the application of hard disk drives[8–10] and memory elements of MRAMs.[11,12] The spin transfer torque (STT), which uses charge transport to influence magnetization, has been exploited to build

STT-MRAM in industry.[5,13] Unlike the traditional MRAMs, which use current-induced Oersted field to switch the magnetization, the STT-MRAM allows a precise control of the magnetization, making the technique much more scalable. A typical STT-MRAM element is a magnetic tunnel junction (MTJ), consisting of a thin insulating tunnel barrier sandwiched by two ferromagnetic thin film electrodes. By passing current through the MTJ, the current gets polarized by one ferromagnetic film and consequently transfers the spin angular momentum that can switch the second ferromagnetic film.[14] The same device can be used for reading out the information encoded in the magnetization through the tunneling magneto resistance.[15,16] A typical memory element based on the STT-MRAM is illustrated in Fig. 1(a).

Very recently, another mechanism has been studied that allows accurate control of the magnetization by deploying the spin–orbit interaction.[17–21] In the case of STT-MRAM, spin–orbit interaction is usually detrimental because it scatters and dissipates the spin angular momentum. However, as it has been shown in numerous studies recently, such spin scattering by the spin–orbit interaction is not completely random. Influenced by the spin–orbit interaction, an in-plane charge current through a ferromagnet (FM)/nonmagnet (NM) bilayer thin film can generate a spin accumulation in a specific direction, which in turn can apply a spin torque on the magnetization of the FM. This spin torque is generally referred to as a spin–orbit torque (SOT), which leads to a new type of memory, SOT-MRAM. In a SOT-MRAM, as shown in Fig. 1(b), the writing current is applied in the film plane, while the readout is via measuring the resistance of the magnetic tunnel junction, similar to that in the STT-MRAM. This architecture separates the write and read currents, which allows independent optimization of the two paths.[1]

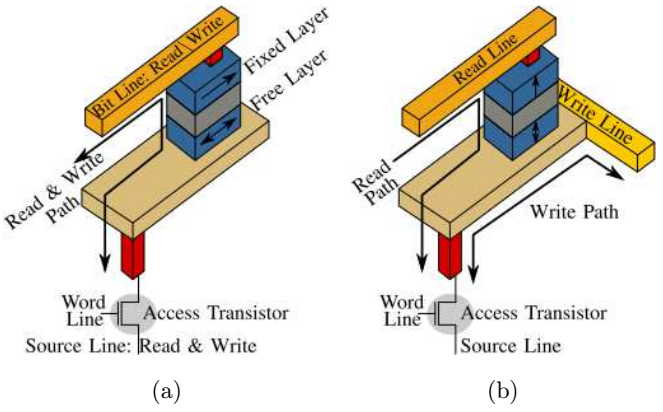

Fig. 1. Bit-cell architecture for (a) STT-MRAM and (b) SOT-MRAM. Adapted from Ref. 1 permission pending.

Besides the application in switching the magnetization, the SOT also has unique applications in efficiently moving magnetic domains much faster than those moved by the current-induced STT.[22–24] The SOT can also be used to drive anti-damping magnetic auto-oscillations,[25] even in devices with an extended size.[26] In this review, we will mainly focus on the application of the SOT in magnetization switching. We will first discuss the possible origins of the SOT and the ongoing debate on the microscopic mechanisms. We then summarize different experimental techniques to measure the SOT. Different novel materials will be reviewed that have the potential to improve the efficiency of SOT-induced magnetization switching. In the end, we will focus specifically on new methods to switch a perpendicularly magnetized film, which is favorable in the application of SOT-MRAMs.

2. Origin of the Spin–Orbit Torques and the Controversies

Although there has been a consensus that the torque generated by an in-plane charge current is due to the spin–orbit interaction, the debate on the type of the spin–orbit interaction has not been fully settled. Taking a FM/NM bilayer as an example, some argue that the SOT is due to the STT from the spin current, which is generated due to the spin Hall effect (SHE) in the bulk of the NM,[27–29] while others argue that it is the interface Rashba–Edelstein effect (REE) that gives rise to the SOT.[30,31]

2.1. *The spin hall effect*

The SHE was firstly discussed by Dyakonov and Perel 40 years ago,[32,33] and reinvigorated by Hirsh.[27] It describes a phenomenon that a charge current through a NM can generate a spin current that is polarized perpendicular to both directions of the charge and spin currents. The SHE can be mathematically described as $\mathbf{Q}_{\boldsymbol{\sigma}} = \frac{\hbar}{2e}\theta_{\mathrm{SH}}\mathbf{j} \times \boldsymbol{\sigma}$, where $\hbar$ is the reduced Planck's constant, e is the charge of an electron, $\mathbf{Q}_{\boldsymbol{\sigma}}$ is the spin current density with the subscript $\boldsymbol{\sigma}$ denotes the spin polarization direction, $\mathbf{j}$ is the charge current density, and θ_{SH} is called the

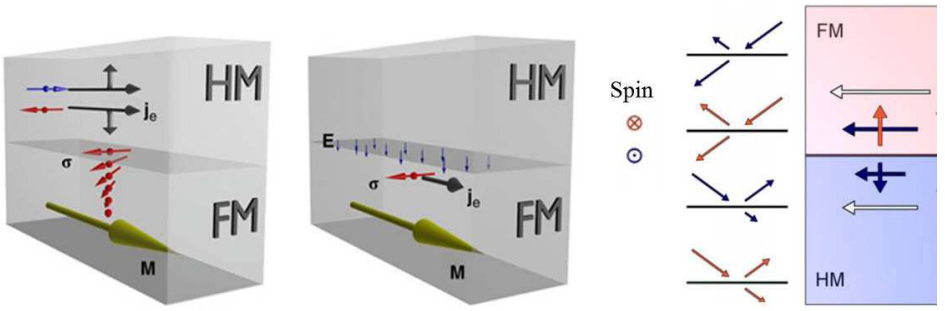

(a) (b) (c)

Fig. 2. (a) Schematics to show the SHE-induced spin torque. Here, the sphere and arrow represent the electron and spin direction, respectively and the grey arrow indicate the electron trajectory. The yellow arrow represent the magnetization direction. HM is a heavy metal, which is equivalent to NM in this paper. Figure adapted from Ref. 38 permission pending. (b) Schematics to illustrate the early picture of REE-induced spin torque. Figure adapted from Ref. 38 permission pending. (c) Schematics to show interlayer spin-dependent scattering-induced spin current. Here white arrows represent the flow of charge. Colored arrows show the flow of spins with spin directions represented by the color as defined in the figure. The length of the arrow indicates the magnitude of scattered spin currents. Figure adapted from Ref. 51 permission pending (color online).

spin Hall angle that describes the efficiency of the charge-to-spin conversion. In the NM/FM bilayer, when a charge current is applied, a spin current can be generated from the SHE in the NM and diffuses toward the FM, as shown in Fig. 2(a). The spin current applies a STT to the magnetization of the FM, which can be expressed as

$$\boldsymbol{\tau}_{\mathrm{DL}} = \frac{\xi_{\mathrm{DL}}|\mathbf{Q}_{\boldsymbol{\sigma}}|}{\mu_0 M_s d_{\mathrm{FM}}} \mathbf{m} \times (\boldsymbol{\sigma} \times \mathbf{m}), \tag{1}$$

where $\mu_0 M_s$ is the saturation magnetization of the FM, d_{FM} is the thickness of the FM, ξ_{DL} is an interface-dependent coefficient that describes the efficiency of the STT. This torque has a similar symmetry dependence on the magnetization as the damping term in the Laudau–Lifshitz equation, and hence is often referred to as the damping-like (DL) torque. In addition, the injection of the spin current may result in a field-like (FL) torque, $\boldsymbol{\tau}_{\mathrm{FL}} = \frac{\xi_{\mathrm{FL}}|\mathbf{Q}_{\boldsymbol{\sigma}}|}{\mu_0 M_s d_{\mathrm{FM}}}(\boldsymbol{\sigma} \times \mathbf{m})$, where ξ_{FL} is the efficiency for the FL torque. The existence of the FL torque in a STT experiment has been a debate.[34,35] An FL torque has been measured to be strong in a magnetic tunnel junction, but very weak in a spin valve.[36,37] This is argued because the FL torque arises from rotation of spins, which is significantly suppressed by dephasing when the spins are noncoherent in the case of spin valves. However, in recent SOT measurements, nonzero FL SOTs are observed in Py/Cu/Pt,[38,39] CoFeB/Cu/Pt,[40] and CoFeB/Hf/W,[41] where the spacer layer separates the FM and the NM with strong spin–orbit interaction. These nonlocal FL torques have been attributed to spin transfer process from spin currents generated in the NM or at the NM/spacer interfaces.[38,42] But they may also be explained by the spin swapping effect,[43,44] which will be discussed next. Difficulty in separating the FL SOT and the current-induced Oersted field in the experiment is also one of the reasons that impedes the understanding of the nonlocal FL SOT.

The magnitude of $\mathbf{Q}_{\boldsymbol{\sigma}}$ in a NM/FM bilayer is often calculated using a drift-diffusion model, where the transport of the spin current in the bulk of the NM is diffusive and the spin current at the NM/FM interface is evaluated using the magneto electric circuit theory.[45–48] For an NM with thickness much greater than its spin diffusion length, the spin current is given by $|\mathbf{Q}_{\boldsymbol{\sigma}}| = \frac{\hbar}{2e}\theta_{\mathrm{SH}} j_e [1 + \frac{\sigma}{2\lambda G^{\uparrow\downarrow}}]^{-1}$,[49,50] where σ is the charge conductivity of the NM, λ is the spin diffusion length in the NM and $G^{\uparrow\downarrow}$ is the interface spin mixing conductance at the NM/FM interface.

2.2. *The Rashba–Edelstein effect*

The REE in the FM/NM was initially described in analogues to that in a two-dimensional electron gas.[30,52–54] Due to the structural inversion symmetry at the interface, an in-plane charge current propagates at the interface experiences an in-plane effective magnetic field perpendicular to the current direction, which results in a spin accumulation $\boldsymbol{\sigma}$ near the interface, as illustrated in Fig. 2(b). Due to the exchange interaction, this spin accumulation

generates an effective FL torque on the magnetization, $\mathbf{T}_{\mathrm{FL}} = \eta_{\mathrm{FL}}(\boldsymbol{\sigma} \times \mathbf{m})$, where η_{FL} is a coefficient to describe the strength of the REE-induced FL torque. In addition, the spin accumulation $\boldsymbol{\sigma}$ will also precess around the magnetization,[55,56] leading to an accumulation of $\mathbf{m} \times \boldsymbol{\sigma}$, which can generate an effective DL torque on the magnetization via exchange interaction, $\mathbf{T}_{\mathrm{DL}} = \eta_{\mathrm{DL}}\mathbf{m} \times (\boldsymbol{\sigma} \times \mathbf{m})$, where η_{DL} is a coefficient to describe the strength of the REE-induced DL torque.

The REE has been theoretically shown to be proportional to another interface spin–orbit interactions, the Dzyaloshinskii–Moriya interaction (DMI).[57,58] The observation of the DMI in bilayer systems like Pt/Co,[59–62] Ta/CoFeB[24,63,64] suggests the existence of the REE. Another signature of the REE-induced SOT is its dependence on the polar angle,[65] which was attributed to the distortion of the Fermi surface by the REE.[66] However, it will require further studies to quantify the exact contribution of the REE-induced SOTs to the overall measured SOTs.

The REE model shown above assumes the electrons are confined near the interface. However, in metallic thin films, electrons can freely scatter among different layers. Recently, Amin *et al.*[51] proposed a new model of the REE-induced SOT by including the three-dimensional electron transport, as depicted in Fig. 2(c). The interface is treated as a spin- and momentum-dependent scattering barrier with energy $E \propto \boldsymbol{\sigma} \cdot (\mathbf{k} \times \mathbf{z})$, which accounts for the REE. Here $\mathbf{k}$ is the wave vector of the electron and $\mathbf{z}$ is the interface normal. Due to the dissimilar band structure and conductivity in the two layers, even without accounting for the magnetization of the FM, electrons scattering at the interface will necessarily lead to a perpendicularly flowing spin current with spin polarized in-plane and perpendicular to the charge current. This effect, sometimes referred to as the interface spin Hall effect,[67] contributes to the SOT very similarly as the SHE except the spin current is generated at the interface. It is difficult to distinguish the SHE and REE even in FM/Cu/NM trilayer because the two share the same symmetry. The main difference in the two mechanisms is that the spin current is generated at the bulk of the NM due to the SHE and near the Cu/NM interface due to the REE. However, in typical NM with strong spin–orbit interactions, e.g., Pt, Ta, the spin diffusion length is found to be very short,[68,69] making it nontrivial to distinguish the SHE and REE by the NM thickness dependence. Recently, Tao *et al.* studied a system of CoFeB/V, where medium magnitude of current-induced SOT is observed.[70] The SOT is found to scale with the spin diffusion length of V, which is about 16 nm. The long-length scale suggests the SHE is a dominant mechanism in this material system. However, the contribution of SHE and REE in bilayers with Pt or Ta as the NM remains unsettled.

It is usually believed that strong spin–orbit interaction is associated with heavy elements. However, as discovered by Emori *et al.*,[42] a sizable FL torque can be observed in $\mathrm{Ti/Py/Al_2O_3}$ even though all the elements are relatively light and no significant SHE has been reported in these layers. Their results suggest that REE may exist at the $\mathrm{Py/Al_2O_3}$ interface even without a heavy element.

2.3. *The spin swapping effect*

Besides the SHE and REE, there is another lesser known mechanism that may be responsible for the SOT in FM/NM bilayer: the spin swapping effect.[43,44] Lifshits and Dyakonov showed that a spin current in a material can generate new spin currents with swapped spin polarization and spin flow directions. The process, as illustrated in Figs. 3(a)–3(c), can be mathematically described as in Ref. 43

$$\mathbf{Q}_{ij}^{\mathrm{new}} = \chi(\mathbf{Q}_{ji}^{\mathrm{original}} - \delta_{ij}\mathbf{Q}_{kk}^{\mathrm{original}}), \tag{2}$$

where the indices $\{i, j\} = \{x, y, z\}$, with the first index denote the spin current flowing direction and the second denote the spin polarization, and χ is a material-dependent coefficient related to the spin–orbit interaction. In a FM/NM bilayer, due to the spin-dependent electron scattering at the FM/NM interface, an in-plane charge current $\mathbf{j}_e$ can induce a flow of spin current parallel to $\mathbf{j}_e$ in the NM with spin polarization parallel to the magnetization of the FM, $\mathbf{m}$, as illustrated in Fig. 3(d). Due to the spin swapping effect, a spin current polarized in direction of $\mathbf{m} \times (\mathbf{z} \times \mathbf{j}_e)$ will be generated in the NM that flows toward the FM. This spin current can also generate a DL torque, which has the same symmetry as the FL SOT generated by the SHE or REE.[44]

It has been theoretically pointed out that when the disorder strength increases in the material, the spin Hall effect increases while the spin swapping effect decreases.[44] This may potentially be the key to

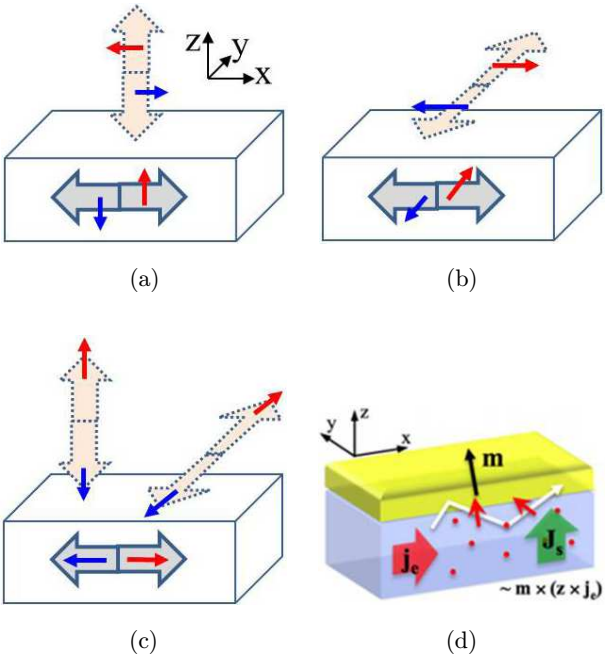

Fig. 3. (a)–(c) Illustration of the spin swapping in different configurations, as described by Eq. (2). (d) Illustration of SOT generated by the spin swapping effect. Adapted from Ref. 44 permission pending.

distinguish the spin swapping effect from other spin–orbit effects.

3. Development in the Measurement Techniques

The common techniques used to measure the current-induced SOT generally fall into four categories: low-frequency electrical measurement, microwave measurement, optical measurement and anti-damping measurement. The first three techniques are based on measuring the small perturbation to the magnetization due to an in-plane applied current. The fourth technique is based on measuring how the applied current changes the damping constant of the FM. Although sometimes the current-induced full magnetization switching is also performed, it complements the perturbation methods by confirming the extracted SOTs are in a reasonable range. However, discrepancy of the SOT is expected since the magnetization switching is a nonlinear process, which is often accompanied by domain nucleation.[71] Here, we first discuss how magnetizations respond to small perturbation of current-induced SOTs, followed by the review of the perturbation methods in three categories and their respective challenges. Then, we will briefly review the anti-damping method.

As shown in Fig. 4(a), an in-plane charge current generates a spin current with spin polarization along $\boldsymbol{\sigma}$ and a spin accumulation at the interface with the same polarization. This in turn applies a damping-like SOT and a field-like SOT on the magnetization. The damping-like SOT, $\gamma M_s h_{\mathrm{DL}} \mathbf{m} \times \boldsymbol{\sigma} \times \mathbf{m}$, can be described as an equivalent field $\gamma h_{\mathrm{DL}} \mathbf{m} \times \boldsymbol{\sigma}$, where γ is the gyromagnetic ratio, M_s is the saturation magnetization, h_{DL} is the magnitude of the equivalent field to the damping-like SOT, $\mathbf{m}$ is the unit vector of the magnetization. The field-like SOT, $M_s h_{\mathrm{FL}} \boldsymbol{\sigma} \times \mathbf{m}$ can be described as an equivalent field $h_{\mathrm{FL}} \boldsymbol{\sigma}$, where h_{FL} is the magnitude of the equivalent field to the field-like SOT. Besides the SOTs, the current can also generate an in-plane Oersted field $h_{\mathrm{Oe\_in}}$, which shares the same symmetry as $h_{\mathrm{FL}} \boldsymbol{\sigma}$ and an out-of-plane Oersted field $h_{\mathrm{Oe\_out}}$. The out-of-plane Oersted field is spatially asymmetric and averages out to be zero.[38] Therefore, in most experiments, its contribution is negligible. The current-induced magnetization reorientation can in general be expressed as

$$\frac{d\mathbf{m}}{dI} = \nabla_h \mathbf{m} \cdot \frac{h_{\mathrm{DL}} \mathbf{m} \times \boldsymbol{\sigma} + h_{\mathrm{FL}} \boldsymbol{\sigma} + h_{\mathrm{Oe\_in}} \boldsymbol{\sigma}}{I}, \quad (3)$$

where ∇_h denotes the gradient with respect to effective magnetic fields.

3.1. *Electrical method*

The typical electrical detection of the SOT is by applying a low frequency current and measuring the Hall voltage response, as shown in Fig. 4(b). The Hall voltage of a magnetic film depends on the magnetization, $V = IR_{\mathrm{AH}} m_z + IR_{\mathrm{PH}} m_x m_y$, where m_x, m_y and m_z are, respectively, the x, y and z component of $\mathbf{m}$, I is the applied current, R_{AH} is the anomalous Hall resistance, and R_{PH} is the planar Hall resistance. The current-induced magnetization reorientation induces a second-order voltage response, $\Delta V = I^2 R_{\mathrm{AH}} \frac{dm_z}{dI} + I^2 R_{\mathrm{PH}} \frac{dm_x}{dI} m_y + I^2 R_{\mathrm{PH}} m_x \frac{dm_y}{dI}$. This second-order voltage response, in combination with Eq. (3) and proper calibration methods, can be used to extrapolate h_{DL} and h_{FL}. Electrical detection is relatively easy to carry out and yields sensitive measurements. However, because the voltage depends on both in-plane and out-of-plane magnetization components due to the coexistence of the anomalous Hall and planar Hall effect, the

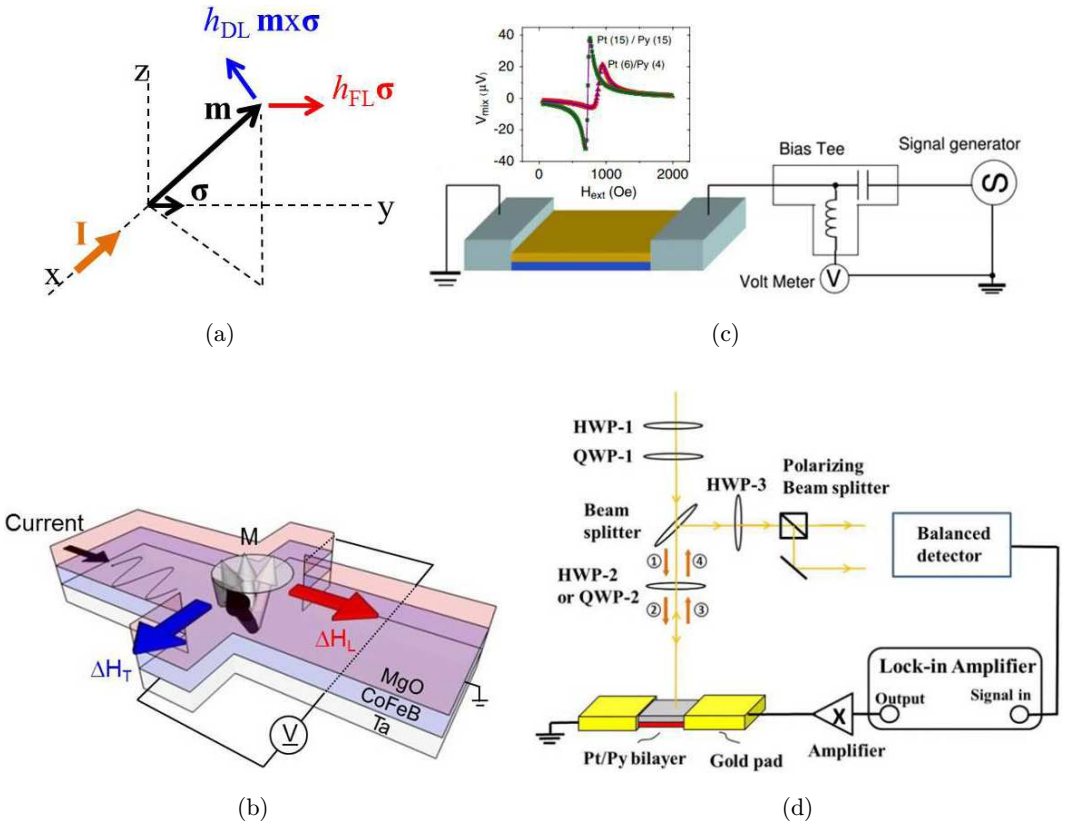

Fig. 4. (a) Illustration of the equivalent fields generated by the current-induced SOTs. (b) Typical electrical measurement of the SOT using a Hall bar structure. Adapted from Ref. 29 permission pending. (c) Setup for measuring the SOT using rectifying voltage at the ferromagnetic resonance. The inset is a typical rectifying voltage measured as a function of a sweeping external magnetic field. Adapted from Ref. 72 permission pending. (d) Setup for measuring the SOT using the MOKE. Adapted from Ref. 73 permission pending.

extrapolation process is rather complicated[65] and sensitive to fitting parameters.[74] In addition, the second-order voltage signal may carry an additional term that is proportional to $I^2 m_x$ due to the anomalous Nernst effect and the spin Seebeck effect[38,75] because the sample gets heated by the applied current. In certain material systems, it has been argued that the planar Hall and thermal contributions are relatively weak, thus the extrapolation process can be significantly simplified. However, caution should be taken when applying the electrical method to a new material system. This method has been widely used to measure SOTs in both in-plane and out-of-plane magnetized samples.[72,76]

3.2. *Microwave method*

When a microwave current is applied through the sample, the current-induced SOTs in concert with an external magnetic field can drive ferromagnetic resonance of the magnetic films. If the magnetization is not parallel with the applied current, the magnetization precession leads to a rectifying effect, giving rise to a dc voltage due to the anisotropic magnetoresistance (AMR), $\Delta V = I^2 \Delta R_{\mathrm{AMR}} \frac{dm_x^2}{dI}$, where ΔR_{AMR} is the resistance difference between the cases where **m** is parallel and perpendicular with the current direction. A typical experimental setup is shown in Fig. 4(c). The voltage signal resembles the ferromagnetic resonance, which can be fitted and used to extrapolate the current-induced SOTs based on Eq. (3). This method is particularly useful for measuring h_{DL} in in-plane magnetized sample. Unlike the low frequency electrical measurement where h_{DL} only induces weak out-of-plane magnetization reorientation, h_{DL} can drive significant in-plane magnetization reorientation at ferromagnetic resonance.[29] Recently, it has also been demonstrated to measure the SOT in out-of-plane magnetized samples.[77]

Because the measurement is done at microwave frequency, a fine tuning of the sample resistance is usually recommended to match the impedance of the microwave transmission line. In addition, calibration of the actual microwave current flowing into the sample is necessary to facilitate the extrapolation of SOTs.[78,79] Since this method measures the longitudinal resistance instead of the Hall resistance, it is not subject to the complication of the entanglement among various components of magnetizations as discussed in the electrical method. However, the precessing magnetization can cause a dc spin pumping voltage,[80] which resembles the ferromagnetic resonance profile and exhibits a similar symmetry as the rectifying voltage due to AMR. In addition, the precessing magnetization may also modify the microwave current flowing through the sample due to the ac spin pumping effect.[81] Recently, a comparison study reports that the SOT measurements in permalloy(Py)/Pt bilayers are consistent using the microwave method and an optical method (will be discussed below),[73] which in principle does not subject to the complication from the spin pumping effect. This suggests that the spin pumping effect may be negligible in the microwave method for Py/Pt bilayer.

3.3. *Optical method*

The magnetization reorientation due to the current-induced SOT can be detected by the magneto-optic-Kerr-effect (MOKE). In a typical measurement setup, as shown in Fig. 4(d), when a linearly polarized or circuit polarized light is perpendicularly incident onto the sample, the magnetization reorientation is translated into the polarization change of the light, which is analyzed by a balanced detector. If a linearly polarized light is used, the polarization change of the light arises from both the polar MOKE and quadratic MOKE effects, $\psi_{\mathrm{Kerr}} = \xi_{\mathrm{Polar}} \cos\theta_M + \xi_{\mathrm{Quad}} \sin^2\theta_M \sin[2(\phi_M - \phi)]$, where ξ_{Polar} and ξ_{Quad} are, respectively, the coefficients for the polar and quadratic MOKE, θ_M and ϕ_M are, respectively, the polar and azimuthal angle of the magnetization, and ϕ is the angle between the linear polarization and the x-axis.[40,73] When the linear light polarization is aligned 45° from the in-plane magnetization direction at equilibrium, i.e., $\phi_M - \phi = 45°$, the current-induced magnetization reorientation will translate to a perturbation to the MOKE response $\Delta\psi_{\mathrm{Kerr}} = I\xi_{\mathrm{Polar}} \frac{dm_z}{dI}$, which is only sensitive to the out-of-plane magnetization reorientation. On the other hand, if a circularly polarized light is used, the polarization of the light is not affected by m_z. Instead, it is only sensitive to the quadratic MOKE, hence the in-plane magnetization reorientation,[73] $\Delta\psi_{\mathrm{Kerr}} = I\xi_{\mathrm{Quad}} \frac{d(m_x m_y)}{dI}$. Through the measurement of the MOKE response and proper calibration, one can extrapolate the SOTs in both in-plane magnetized and out-of-plane magnetized films. Unlike the electrical and microwave measurements, which detect second-order responses, this optical method is based on a first-order perturbation, hence free of complication from the thermal effect.

3.4. *Anti-damping method*

Besides measuring the perturbation on the magnetization due to SOTs, one can also measure SOTs in a FM/NM bilayer by how a dc current can modify ferromagnetic resonance conditions of the FM. In this measurement, the spin polarization is parallel/antiparallel with the magnetization, which generates a DL torque enhancing/opposing the damping torque and a FL torque that acts as an in-plane effective field.[29,42,82] These two effects give rise to change of damping and shifts the resonance field, respectively, from which one can extrapolate the current-induced SOTs.

While all these methods have been demonstrated to be sensitive, there remains a difficulty to distinguish h_{FL} and the in-plane Oersted field because the two generally have the same symmetry. The typical treatment to extrapolate h_{FL} is by estimating the Oersted field from the current distribution based on parallel circuit model.[38]

4. Novel Materials and Structural Engineering for the Application of Spin–Orbit Torque

Many new materials have been developed and investigated to improve the efficiency for magnetization switching by current-induced SOT. We will first review different materials for the NM, including doped metal and alloys,[83,84] rare earth elements,[85] topological insulators[78] and transition metal dichalcogenides.[86] There is also a recent effort in engineering FM to facilitate magnetization switching by using ferrimagnets near the compensation point.[87,88] In addition, the material structure to

improve the efficiency of spin absorption will also be reviewed.[89–91]

4.1. *Metals, alloys and structural engineering*

Besides the 5d heavy metals Pt,[29,82] Ta,[20] W,[92] Hf[93] etc., which have been intensively investigated by the spintronics community, work has shown that impurity induced extrinsic scattering could produce large spin Hall effect.[94–96] Cu alloy with 10% Ir doping has been applied in a three-terminal MTJ device to reduce the threshold current of magnetic switching process.[97] Comprehensive studies of large SOTs in CuAu/FM heterostructures have been carried out by both the second harmonic[83] and the MOKE measurements.[84] It has also been shown that the spin torque efficiency could be substantially enhanced by alloying Pt with Al or Hf.[98]

Recently, some 3D light transition metals have also been demonstrated to have large spin Hall angles.[99,100] The spin orbit torque in vanadium films has been characterized by using the optical method,[70] where a large spin torque efficiency, comparable with Pt, has been obtained in the sputter-deposited CoFeB/V bilayer structures. Meanwhile, the spin torque efficiency of four rare-earth metals, Gd, Dy, Ho and Lu, has been reported by both the ST-FMR experimental measurements and density-functional theory theoretical calculations,[85] which indicates the spin torque efficiency is enhanced by the partially filled f orbitals.

Besides choosing different NM, there is also another strategy to manipulate the spin–orbit torques by structural engineering. For example, the SOTs controlled by the oxygen level manipulation in the CoFeB layer[90] induced a new SOT mechanism that is two times stronger than bulk spin Hall effect. The incorporation of oxygen in W films could introduce a large spin Hall angles of up to -0.5 in the W(O)/CoFeB/TaN structure.[89] It has also been shown that natural oxidation in Cu could lead to significantly enhanced SOTs, even though Cu is supposed to have weak spin–orbit coupling.[91]

Since the SOTs due to both the SHE and REE depend on interface, it is possible to improve the SOT by interface engineering. Pai *et al.*[101] showed that the SOT due to the SHE depends on the interface transparency of the spin current in Pt/FM bilayer. Weifeng Zhang *et al.* demonstrated that the SOT can be enhanced in Pt/Py bilayer by adding a thin layer of Co at the interface.[49] A strong enhancement of the anti-damping spin torque has also been realized by insertion of the Hf atomic layer between Pt and CoFeB.[102]

4.2. *Topological insulator*

As one of the most promising candidates in the application of SOT devices, topological insulator (TI)[103–105] has several protentional advantages in theory. (1) Large spin torque efficiency: time reversal invariant symmetry protected TI surface state is governed by helical Dirac nature of spin momentum locking, which makes it highly efficient for the generation of spin current.[106–109] (2) Elimination of the charge dissipation: the backscattering process is fully eliminated by the topological protected surface state in TIs (topological protection). The high mobility surface can be used as conduction channels with low joule heating.[110–114] (3) Potential application in energy efficient gate controlled SOT logic devices: Electrical field manipulation of spin polarized surface current could be potentially realized by the nearly linear E–k dispersion of Dirac transport feature.[103,105,115]

As shown in Fig. 5, the current-induced SOTs have been probed by the ST-FMR in Bi_2Se_3/NiFe bilayer system at room temperature[78] and in Figs. 6(a) and 6(b), the surface state contribution has been found to dominate the SOTs at low temperature.[79] The charge-current conversion efficiency is greater than that of any other reported heavy metal, which has potential importance for SOT device applications. In Ref. 116, even greater SOTs have been demonstrated in magnetically doped topological insulator, and the current-induced SOTs assisted magnetic switching has been carried out by low critical current density of $8.9\text{E}{+4}\,\text{A/cm}^2$. Figures 6(c) and 6(d) have shown the current induced spin torque switching at 1.9 K in the presence of an in-plane external magnetic field.

The efficiency of charge to spin-current conversion in TIs has been evaluated quantitatively as a function of the Fermi level position by ST-FMR torque measurement[117] and spin-polarized tunneling technique.[118] The spin-current conversion ratio varies smoothly as the Fermi level position is tuned through the bandgap. Furthermore, in Ref. 119, the carrier density at the Cr-doped TI surface has been effectively modulated by the top gate voltage, and the SOT-assisted magnetization switching has also

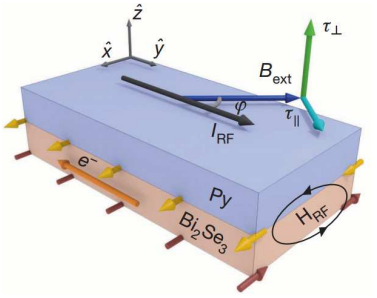

Parameter	Bi_2Se_3 (this work)	Pt (ref. 4)	β-Ta (ref. 6)	Cu(Bi) (ref. 23)	β-W (ref. 24)
$\theta_\parallel$	2.0–3.5	0.08	0.15	0.24	0.3
$\sigma_{S,\parallel}$	1.1–2.0	3.4	0.8	—	1.8

$\theta_\parallel$ is dimensionless and the units for $\sigma_{S,\parallel}$ are $10^5\hbar/2e\ \Omega^{-1}\,m^{-1}$.

Fig. 5. The ST-FMR measurement of the permalloy/Bi_2Se_3. The antidumping-like spin torque ratio was determined as 2 to 3.5 at room temperature which is much larger than any other reported HMs. Adapted from Ref. 78 permission pending.

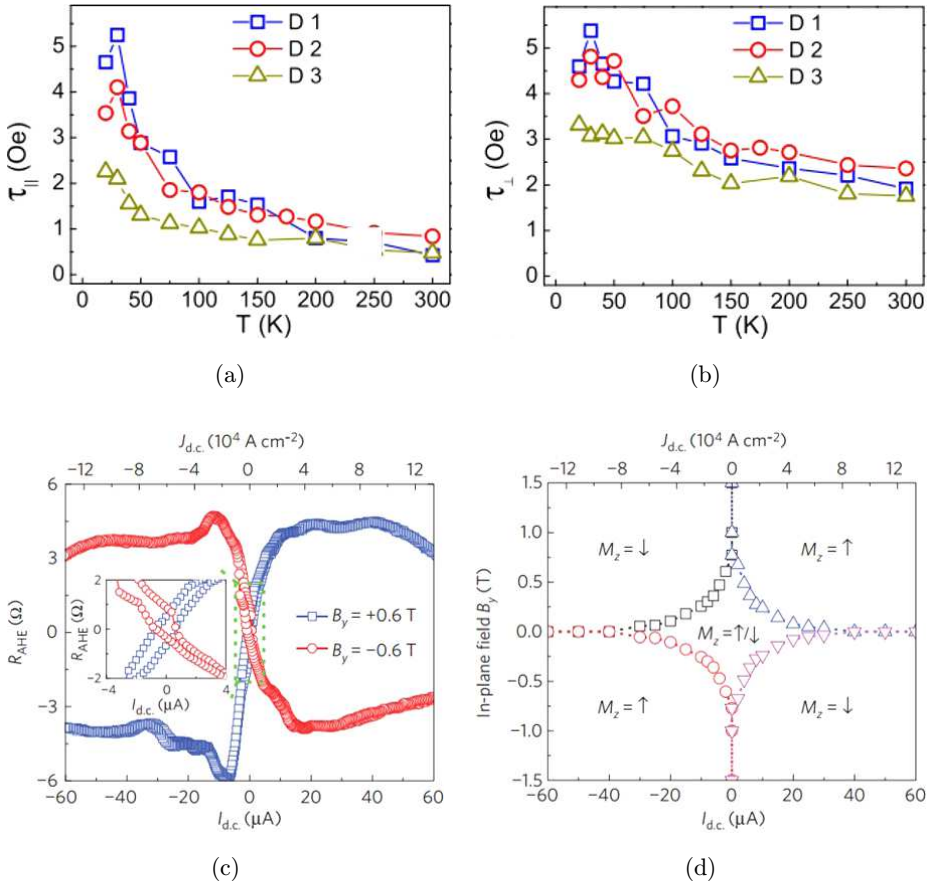

Fig. 6. Temperature dependent measurements of (a) in-plane torque and (b) out-of-plane torque of Bi_2Se_3/CoFeB using the ST-FMR. Adapted from Ref. 79 permission pending. (c) Low temperature current induced spin–orbit torque magnetic switching and phase diagram of magnetic state of $(Bi_{0.5}Sb_{0.5})_2Te_3/(Cr_{0.08}Bi_{0.54}Sb_{0.38})_2Te_3$. Adapted from Ref. 116 permission pending.

been demonstrated by the scanning gate voltage. These findings pave the way to realize highly efficient spintronics logical devices.

It is challenging to integrate the TI-based structures with conventional semiconductor industry process. Recent effort has been devoted to optimizing TI materials for the practical application of room temperature spintronics devices. Recently, both transition metal rare earth ferromagnetic alloys and perpendicularly magnetized CoFeB multilayers have been successfully prepared on TIs by magnetron sputtering.[120,121] The low critical current density[121] has been applied in the magnetization switching experiments, which is much smaller than the typical values in the heavy metal/FM structures.

4.3. *Transition metal dichalcogenide*

Besides the topological insulators, monolayer transition metal dichalcogenide (TMD), which has both strong spin orbit coupling and inversion symmetry breaking, is estimated to have spin momentum locking feature as well. Large SOTs could be potentially generated in a TMD/FM bilayer system.[122–124]

A large damping-like torque has been observed in MoS_2/Py bilayers by the ST-FMR measurement[125] (the origin of the large spin torque hasn't been fully discussed). In studies of both MoS_2/CoFeB and WSe_2/CoFeB bilayers, field-like SOTs are found to dominate damping-like SOTs in the TMD/CoFeB system, which is attributed to the REE. The strong spin orbit coupling and intrinsic inversion symmetry breaking give rise to this large Rashba–Edelstein effect.[126]

4.4. *Ferrimagnets*

Besides improving the charge-to-spin conversion efficiency in the NM and engineering the NM/FM interface, the magnetization switching condition can also be tuned by choosing different FMs. In ferrimagnets such as CoGd[87] and CoTb,[88] magnetic moments of rare-earth element and 3D transition element are antiparallelly aligned. Therefore, by tuning the composition, one can obtain a ferrimagnet near compensation point with a very low saturation magnetization. Since the SOT inversely scales with the magnetization, low threshold current is expected to switch the magnetization of such a ferrimagnet.[87,120]

5. Switching Perpendicular Magnetization

In the application of magnetic memories, perpendicular magnetization is more favorable over in-plane magnetization due to better scalability and stability.[11,127] In the STT-based MRAMs, perpendicular magnetization can be efficiently switched by the injection of perpendicularly polarized spin current across a tunnel barrier, which can be generated via the spin filtering effect from the second perpendicularly magnetized layer.[5] However, efficient switching of perpendicular magnetization remains a conundrum in the SOT-based MRAMs. This is because the spin current that flows into the magnetic film is usually polarized in the film plane only, which is limited by the thin film geometry and the symmetry of the conventional spin–orbit interaction. In order to switch a perpendicular magnetization with an in-plane polarized spin current, additional symmetry in the system has to be broken. The first demonstration of perpendicular magnetization switching with SOT is performed by Miron *et al.*,[18] where an external magnetic field is applied to tilt the magnetization away from the nominal perpendicular direction. Since it is impractical to switch a perpendicular magnetization with the assistance of an external magnetic field, several groups have reported external field-free switching by using a built-in in-plane exchange fields.[128,129]

Garello *et al.*[130] have experimentally demonstrated that it is possible to switch a perpendicular magnetization with a current pulse of 200 ps, much shorter than the typical switching time of STT-based magnetic memories. While the fast switching speed makes this switching mechanism very appealing, the down side is that during the switching, the SOT competes against the anisotropy, which requires a higher energy input than the STT-induced switching where the STT competes against the damping. It is important to emphasize that the difference between the SOT- and STT-induced switching is not due to the different origin of the spin current, but rather because of the polarization direction of the spin current. In the STT-induced perpendicular magnetization switching, by purposely including an in-plane reference magnetic layer in a double-barrier magnetic tunnel junction, one can also generate an in-plane polarized spin current, which has been used to accelerate the switching process.[131,132]

5.1. *Generation of perpendicularly polarized spin current with the spin–orbit effects*

A perpendicularly polarized spin current can switch a perpendicular magnetization without the assistance of any in-plane field. In this switching process, the SOT competes again with the anisotropy. In order to efficiently switch a perpendicular magnetization via the anti-damping process, one needs to generate a perpendicularly polarized spin current. However, in a standard FM/NM bilayer without additional symmetry breaking, it is forbidden by symmetry for an in-plane charge current to generate a perpendicularly flowing spin current with perpendicular spins,

which is articulated by MacNeil *et al.*[133] If an in-plane charge current could generate a perpendicular spin polarization, reversing the charge current is equivalent to rotating the sample at 180°. The former will lead to a reverse of the spin polarization but the latter will yield the same spin polarization. Therefore, the perpendicular spin polarization generated by an in-plane charge current must be zero.

In order to generate perpendicularly polarized spin current, one needs to resort to additional symmetry breaking besides the spin–orbit interactions. Very recently, MacNeil *et al.* demonstrated that an out-of-plane SOT can be generated from an in-plane charge current in a WTe_2/Py bilayer. As shown in Fig. 7(a), the WTe_2 lacks the mirror symmetry in the b-c plane, which is parallel to the Py thin film plane. This additional symmetry breaking allows the generation of perpendicular spin torque, which can potentially be used to switch a perpendicular magnetization via anti-damping switching.

Besides the special crystal structures, magnetic ordering can also be explored to give an additional symmetry breaking that leads to the generation of spin current with unconventional symmetries. Taniguchi proposed that a perpendicularly polarized spin current can be generated using a ferromagnetic film with out-of-plane tilted magnetization, as illustrated in Fig. 7(b). While a charge current can generate an in-plane polarized spin current due to the spin Hall effect in the FM, the transverse spins to the magnetization are subject to quick dephasing.[69,135] This results in a spin filtering effect[134] such that the spin current is polarized parallel with the magnetization, and hence carries a perpendicular component. This mechanism is based on the premise that the transverse spins in a FM are much more significantly suppressed than longitudinal spins. However, recently, Humphries *et al.* have shown that the spin–orbit effects of transverse spins are not necessarily trivial in a FM. If the dephasing does not completely suppress transverse spins, the precession of spins around the magnetization leads to the generation of spin current in an unexpected symmetry.[136] It is experimentally demonstrated

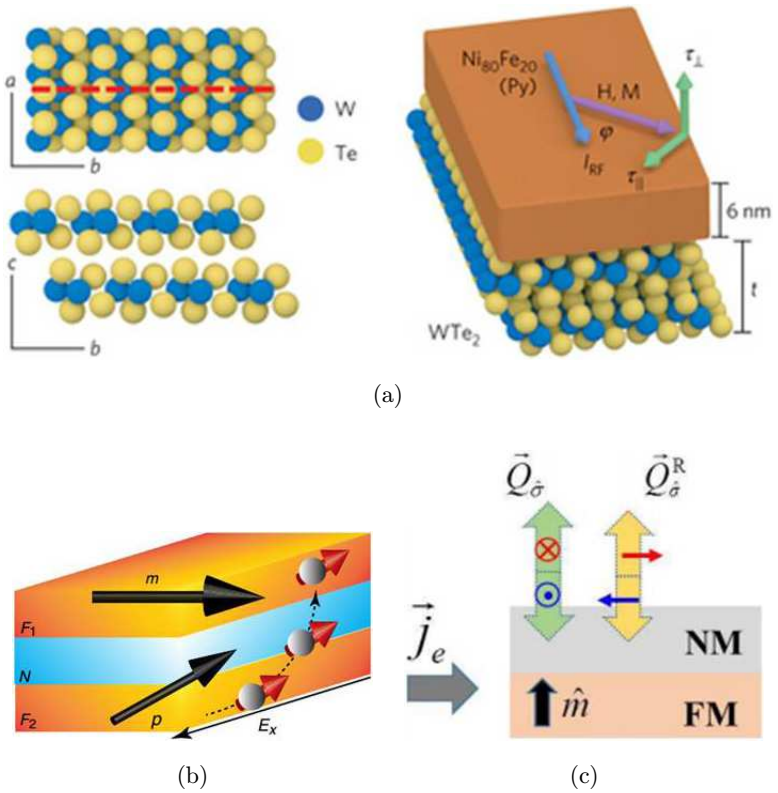

Fig. 7. (a) Structure of the WTe_2 for generating perpendicularly polarized spin current, Adapted from Ref. 133 permission pending. (b) Structure for generating perpendicularly polarized spin current from the anomalous Hall effect and spin filtering, Adapted from Ref. 134 permission pending. (c) Structure for demonstrating spin–orbit effect with spin rotation. In this figure, $\mathbf{Q}_{\hat{\sigma}}$ is the spin current with conventional symmetry, while $\mathbf{Q}^R_{\hat{\sigma}}$ is the spin current with spin rotation symmetry.

that an in-plane charge current in a perpendicularly magnetized multilayer film can generate a perpendicularly flowing spin current with polarization parallel to the charge current, as shown in Fig. 7(c). This suggests that an in-plane charge current through an in-plane magnetized film may generate a perpendicularly flowing spin current with perpendicular spin component that may be useful for switching a perpendicular magnetization.

6. Conclusion

Spin–orbit effects in magnetic multilayers are at the heart of spintronics research. Here we only give a brief review on the current-induced spin–orbit torques in metallic multilayers. Its reverse effect, the conversion of spin current to charge current, is also being actively studied. These two venues of studying the spin–orbit effects complement each other and pave a road to novel applications. Recently, it is also demonstrated that the SOT can manipulate antiferromagnetic ordering,[137] which creates a new possibility for information storage using antiferromagnets.

While it is crucial to understand the origin of the spin–orbit effects, distinguishing the bulk spin Hall effect and the interface Rashba–Edelstein effect remains a conundrum. This is because they have the same symmetries with respect to magnetization orientation and sample stacking order as well as similar thickness-dependence. Various experimental techniques have been developed and refined to allow the measurement of the SOTs at a high sensitivity. However, it will take a collective effort from both experimentalists and theorists to separate the different contributions to the SOTs.

The end goal of the SOT study is to develop a material system that allows the control of magnetization with very small amount of current. Along that line, various materials with exotic spin–orbit interactions have been explored as the NM. There is also a parallel effort in studying the FM to increase the efficiency of the SOT by lowering the saturation magnetization. In addition, interface engineering can also help improve the SOT efficiency.

Through fundamental researches to settle the controversial debate, better understanding of the spin–orbit effects can be achieved to guide the design for potential applications. As the field progresses, we expect to see more exciting discoveries on the way.

Acknowledgment

This work at the University of Delaware was supported by the National Science Foundation under Grant Numbers DMR-1505192, and that at the University of Denver was supported by the NSF Grant ECCS-1738679.

References

1. F. Oboril, R. Bishnoi, M. Ebrahimi and M. B. Tahoori, *IEEE Trans. Comput. Des. Integr. Circuits Syst.* **34**, 367 (2015).
2. S. S. P. Parkin *et al.*, *J. Appl. Phys.* **85**, 5828 (1999).
3. J.-G. Zhu, Y. Zheng and G. A. Prinz, *J. Appl. Phys.* **87**, 6668 (2000).
4. C. Chappert, A. Fert and F. N. Van Dau, *Nat. Mater.* **6**, 813 (2007).
5. D. Apalkov *et al.*, *ACM J. Emerg. Technol. Comput. Syst.* **9**, 1 (2013).
6. M. N. Baibich *et al.*, *Phys. Rev. Lett.* **61**, 2472 (1988).
7. G. Binasch, P. Grünberg, F. Saurenbach and W. Zinn, *Phys. Rev. B* **39**, 4828 (1989).
8. C. Tsang *et al.*, *IEEE Trans. Magn.* **30**, 3801 (1994).
9. G. A. Prinz, *Science* **282**, 1660 (1998).
10. S. A. Wolf *et al.*, *Science* **294**, 1488 (2001).
11. N. Nishimura *et al.*, *J. Appl. Phys.* **91**, 5246 (2002).
12. S. Tehrani *et al.*, *Proc. IEEE* **91**, 703 (2003).
13. Y. Huai, *AAPPS Bull.* **18**, 33 (2008).
14. D. C. Ralph and M. D. Stiles, *J. Magn. Magn. Mater.* **320**, 1190 (2008).
15. T. Miyazaki and N. Tezuka, *J. Magn. Magn. Mater.* **139**, L231 (1995).
16. J. S. Moodera, L. R. Kinder, T. M. Wong and R. Meservey, *Phys. Rev. Lett.* **74**, 3273 (1995).
17. P. Gambardella and I. M. Miron, *Philos. Trans. R. Soc. A Math. Phys. Eng. Sci.* **369**, 3175 (2011).
18. I. M. Miron *et al.*, *Nature* **476**, 189 (2011).
19. L. Liu, O. J. Lee, T. J. Gudmundsen, D. C. Ralph and R. A. Buhrman, *Phys. Rev. Lett.* **109**, 96602 (2012).
20. L. Liu *et al.*, *Science* **336**, 555 (2012).
21. K. Jabeur, L. D. Buda-Prejbeanu, G. Prenat and G. D. Pendina, *Int. J. Electron. Sci. Eng.* **7**, 501 (2013).
22. P. P. J. Haazen *et al.*, *Nat. Mater.* **12**, 299 (2013).
23. K.-S. Ryu, L. Thomas, S.-H. Yang and S. Parkin, *Nat. Nanotechnol.* **8**, 527 (2013).
24. S. Emori, U. Bauer, S.-M. Ahn, E. Martinez and G. S. D. Beach, *Nat. Mater.* **12**, 611 (2013).
25. S. Urazhdin, V. Tiberkevich and A. Slavin, *Phys. Rev. Lett.* **105**, 237204 (2010).

26. Z. Duan *et al.*, *Nat. Commun.* **5**, 5616 (2014).
27. J. E. Hirsch, *Phys. Rev. Lett.* **83**, 1834 (1999).
28. S. Zhang, *Phys. Rev. Lett.* **85**, 393 (2000).
29. L. Liu, T. Moriyama, D. C. Ralph and R. A. Buhrman, *Phys. Rev. Lett.* **106**, 36601 (2011).
30. Y. A. Bychkov and E. I. Rashba, *JETP Lett.* **39**, 78 (1984).
31. J. Sinova *et al.*, *Phys. Rev. Lett.* **92**, 126603 (2004).
32. M. I. D'yakonov and V. I. Perel', *JETP Lett.* **13**, 467 (1971).
33. M. I. Dyakonov and V. I. Perel, *Phys. Lett. A* **35**, 459 (1971).
34. S. Zhang, P. M. Levy and A. Fert, *Phys. Rev. Lett.* **88**, 236601 (2002).
35. J. Zhang, P. Levy, S. Zhang and V. Antropov, *Phys. Rev. Lett.* **93**, 256602 (2004).
36. M. A. Zimmler *et al.*, *Phys. Rev. B* **70**, 184438 (2004).
37. J. C. Sankey *et al.*, *Nat. Phys.* **4**, 67 (2007).
38. X. Fan *et al.*, *Nat. Commun.* **4**, 1799 (2013).
39. T. Nan *et al.*, *Phys. Rev. B* **91**, 214416 (2015).
40. X. Fan *et al.*, *Nat. Commun.* **5**, 1 (2014).
41. Y. Ou, C.-F. Pai, S. Shi, D. C. Ralph and R. A. Buhrman, *Phys. Rev. B* **94**, 140414 (2016).
42. S. Emori *et al.*, *Phys. Rev. B* **93**, 180402 (2016).
43. M. B. Lifshits and M. I. Dyakonov, *Phys. Rev. Lett.* **103**, 186601 (2009).
44. H. B. M. Saidaoui and A. Manchon, *Phys. Rev. Lett.* **117**, 36601 (2016).
45. Y. Tserkovnyak, A. Brataas and G. Bauer, *Phys. Rev. Lett.* **88**, 117601 (2002).
46. A. Brataas, Y. Tserkovnyak, G. E. W. Bauer and B. I. Halperin, *Phys. Rev. B* **66**, 60404 (2002).
47. Y. Tserkovnyak, A. Brataas, G. E. W. Bauer and B. I. Halperin, *Rev. Mod. Phys.* **77**, 1375 (2005).
48. Y.-T. Chen *et al.*, *Phys. Rev. B* **87**, 144411 (2013).
49. W. Zhang, W. Han, X. Jiang, S.-H. Yang and S. P. Parkin, *Nat. Phys.* **11**, 496 (2015).
50. M.-H. Nguyen, D. C. Ralph and R. A. Buhrman, *Phys. Rev. Lett.* **116**, 126601 (2016).
51. V. P. Amin and M. D. Stiles, *Phys. Rev. B* **94**, 104420 (2016).
52. Y. A. Bychkov and E. I. Rashba, *J. Phys. C Solid State Phys.* **17**, 6039 (1984).
53. A. Manchon and S. Zhang, *Phys. Rev. B* **78**, 212405 (2008).
54. A. Manchon and S. Zhang, *Phys. Rev. B* **79**, 94422 (2009).
55. A. Manchon, arXiv e-prints 1204.4869 (2012).
56. P. M. Haney, H.-W. Lee, K.-J. Lee, A. Manchon and M. D. Stiles, *Phys. Rev. B* **87**, 174411 (2013).
57. K.-W. Kim, H.-W. Lee, K.-J. Lee and M. D. Stiles, *Phys. Rev. Lett.* **111**, 216601 (2013).
58. A. Kundu and S. Zhang, *Phys. Rev. B* **92**, 94434 (2015).
59. A. Hrabec *et al.*, *Phys. Rev. B* **90**, 20402 (2014).
60. S. Pizzini *et al.*, *Phys. Rev. Lett.* **113**, 47203 (2014).
61. K. Di *et al.*, *Phys. Rev. Lett.* **114**, 47201 (2015).
62. M. Belmeguenai *et al.*, *Phys. Rev. B* **91**, 180405 (2015).
63. J. Cho *et al.*, *Nat. Commun.* **6**, 7635 (2015).
64. X. Ma *et al.*, *Phys. Rev. B* **94**, 180408 (2016).
65. K. Garello *et al.*, *Nat. Nanotechnol.* **8**, 587 (2013).
66. K.-S. Lee *et al.*, *Phys. Rev. B* **91**, 144401 (2015).
67. L. Wang *et al.*, *Phys. Rev. Lett.* **116**, 196602 (2016).
68. L. Liu, R. A. Buhrman and D. C. Ralph, arXiv e-prints 1111.3702 (2011). doi:10.1088/1751-8113/44/8/085201.
69. A. Ghosh, S. Auffret, U. Ebels and W. E. Bailey, *Phys. Rev. Lett.* **109**, 127202 (2012).
70. T. Wang *et al.*, *Sci. Rep.* **7**, 1306 (2017).
71. C.-F. Pai, M. Mann, A. J. Tan and G. S. D. Beach, *Phys. Rev. B* **93**, 144409 (2016).
72. J. Kim *et al.*, *Nat. Mater.* **12**, 240 (2012).
73. X. Fan *et al.*, *Appl. Phys. Lett.* **109**, 122406 (2016).
74. Y. Chen *et al.*, *Phys. Rev. B* **95**, 144405 (2017).
75. C. O. Avci *et al.*, *Phys. Rev. B* **90**, 224427 (2014).
76. M. Hayashi, J. Kim, M. Yamanouchi and H. Ohno, *Phys. Rev. B* **89**, 144425 (2014).
77. A. Kumar *et al.*, *Phys. Rev. B* **95**, 64406 (2017).
78. A. R. Mellnik *et al.*, *Nature* **511**, 449 (2014).
79. Y. Wang *et al.*, *Phys. Rev. Lett.* **114**, 257202 (2015).
80. K. Kondou *et al.*, *Appl. Phys. Exp.* **9**, 23002 (2016).
81. F. S. M. Guimarães *et al.*, arXiv e-prints 1703.04493 (2017).
82. K. Ando *et al.*, *Phys. Rev. Lett.* **101**, 36601 (2008).
83. Y. Wen *et al.*, *Phys. Rev. B* **95**, 104403 (2017).
84. J. Wu *et al.*, *IEEE Trans. Magn.* **52**, 1 (2016).
85. N. Reynolds *et al.*, *Phys. Rev. B* **95**, 64412 (2017).
86. D. MacNeill *et al.*, *Nat. Phys.* **13**, 300 (2016).
87. R. Mishra *et al.*, *Phys. Rev. Lett.* **118**, 167201 (2017).
88. J. Finley and L. Liu, *Phys. Rev. Appl.* **6**, 54001 (2016).
89. K.-U. Demasius *et al.*, *Nat. Commun.* **7**, 10644 (2016).
90. X. Qiu *et al.*, *Nat. Nanotechnol.* **10**, 333 (2015).
91. H. An, Y. Kageyama, Y. Kanno, N. Enishi and K. Ando, *Nat. Commun.* **7**, 13069 (2016).
92. C.-F. Pai *et al.*, *Appl. Phys. Lett.* **101**, 122404 (2012).
93. R. Ramaswamy, X. Qiu, T. Dutta, S. D. Pollard and H. Yang, *Appl. Phys. Lett.* **108**, 202406 (2016).
94. Y. Niimi *et al.*, *Phys. Rev. Lett.* **106**, 126601 (2011).
95. Y. Niimi *et al.*, *Phys. Rev. Lett.* **109**, 156602 (2012).
96. P. Laczkowski *et al.*, *Appl. Phys. Lett.* **104**, 142403 (2014).
97. M. Yamanouchi *et al.*, *Appl. Phys. Lett.* **102**, 212408 (2013).

98. M.-H. Nguyen, M. Zhao, D. C. Ralph and R. A. Buhrman, *Appl. Phys. Lett.* **108**, 242407 (2016).
99. C. Du, H. Wang, F. Yang and P. C. Hammel, *Phys. Rev. B* **90**, 140407 (2014).
100. D. Qu, S. Y. Huang and C. L. Chien, *Phys. Rev. B* **92**, 20418 (2015).
101. C.-F. Pai, Y. Ou, D. C. Ralph and R. A. Buhrman, *Phys. Rev. B* **92**, 64426 (2015).
102. M.-H. Nguyen, K. X. Nguyen, D. A. Muller, D. C. Ralph and R. A. Buhrman, *Appl. Phys. Lett.* **106**, 222402 (2015).
103. M. Z. Hasan and C. L. Kane, *Rev. Mod. Phys.* **82**, 3045 (2010).
104. J. E. Moore, *Nature* **464**, 194 (2010).
105. X. L. Qi and S. C. Zhang, *Rev. Mod. Phys.* **83**, 1057 (2011).
106. A. A. Burkov and D. G. Hawthorn, *Phys. Rev. Lett.* **105**, 66802 (2010).
107. D. Culcer, E. H. Hwang, T. D. Stanescu and S. Das Sarma, *Phys. Rev. B* **82**, 155457 (2010).
108. D. Pesin and A. H. MacDonald, *Nat. Mater.* **11**, 409 (2012).
109. M. H. Fischer, A. Vaezi, A. Manchon and E.-A. Kim, *Phys. Rev. B* **93**, 125303 (2016).
110. M. Konig *et al.*, *Science* **318**, 766 (2007).
111. D. Hsieh *et al.*, *Nature* **452**, 970 (2009).
112. X.-L. Qi and S.-C. Zhang, *Phys. Today* **63**, 33 (2010).
113. K. He *et al.*, *Nat. Phys.* **6**, 584 (2010).
114. Y. P. Chen, Topological insulator-based energy efficient devices, in *Proc. SPIE 8373, Micro- and Nanotechnology Sensors, Systems and Applications IV*, 83730B (May 1, 2012), doi: 10.1117/12.920513.
115. V. M. Edelstein, *Solid State Commun.* **73**, 233 (1990).
116. Y. Fan *et al.*, *Nat. Mater.* **13**, 699 (2014).
117. K. Kondou *et al.*, *Nat. Phys.* **12**, 1027 (2016).
118. L. Liu *et al.*, *Phys. Rev. B* **91**, 235437 (2015).
119. Y. Fan *et al.*, *Nat. Nanotechnol.* **11**, 352 (2016).
120. J. Han *et al.*, arXiv e-prints 1703.07470 (2017).
121. M. Dc *et al.*, arXiv e-prints 1703.03822.
122. D. Xiao, G.-B. Liu, W. Feng, X. Xu and W. Yao, *Phys. Rev. Lett.* **108**, 196802 (2011).
123. X. Xu, W. Yao, D. Xiao and T. F. Heinz, *Nat. Phys.* **10**, 343 (2014).
124. A. Manchon, H. C. Koo, J. Nitta, S. M. Frolov and R. A. Duine, *Nat Mater* **14**, 871 (2015).
125. W. Zhang *et al.*, *APL Mater.* **4**, 32302 (2016).
126. Q. Shao *et al.*, *Nano Lett.* **16**, 7514 (2016).
127. M. Gajek *et al.*, *Appl. Phys. Lett.* **100**, 132408 (2012).
128. Y. Lau, D. Betto, K. Rode, J. M. D. Coey and P. Stamenov, *Nat. Nanotechnol.* **11**, 758 (2016).
129. S. Fukami, C. Zhang, S. DuttaGupta, A. Kurenkov and H. Ohno, *Nat. Mater.* **15**, 535 (2016).
130. K. Garello *et al.*, *Appl. Phys. Lett.* **105**, 212402 (2014).
131. H. Liu *et al.*, *Appl. Phys. Lett.* **97**, 242510 (2010).
132. H. Liu, D. Bedau, D. Backes, J. A. Katine and A. D. Kent, *Appl. Phys. Lett.* **101**, 32403 (2012).
133. D. MacNeill *et al.*, *Nat. Phys.* **13**, 300 (2016).
134. T. Taniguchi, J. Grollier and M. D. Stiles, *Phys. Rev. Appl.* **3**, 44001 (2015).
135. M. D. Stiles and A. Zangwill, *Phys. Rev. B* **66**, 14407 (2002).
136. A. M. Humphries *et al.*, arXiv e-prints 1704.08998 (2017).
137. P. Wadley *et al.*, *Science* **351**, 587 (2016).